Some Predictions on Behavior of the Nuclear Matter in Nuclear Collisions at FAIR-GSI Energies

Nicolae George Țuțuraș * , Alexandru Jipa * , Dănuț Argintaru , Oana Ristea , Marius Călin , Cătălin Ristea , Ionel Lazanu , Tiberiu Eșanu , Adam Jinaru , Murat Ablai

Posted Date: 21 April 2026

doi: 10.20944/preprints202604.1449.v1

Keywords: hadronic gas; K^+ mesons; anisotropic flow; resonance matter; particle ratios

 doi:10.20944/preprints202604.1449.v1

Article

Some Predictions on Behavior of the Nuclear Matter in Nuclear Collisions at FAIR-GSI Energies

Nicolae George Ţuţuraş [1,*], Alexandru Jipa [1,*], Dănuț Argintaru [2], Oana Ristea [1], Marius Călin [1], Cătălin Ristea [3], Ionel Lazanu [1], Tiberiu Eşanu [4], Adam Jinaru [4] and Murat Ablai [1]

[1] Faculty of Physics, University of Bucharest, Bucharest, Romania
[2] Constanţa Maritime University, Constanţa, Romania
[3] Institute of Space Science, Bucharest-Măgurele, Romania
[4] Horia Hulubei National Institute for R&D in Physics and Nuclear Engineering, Bucharest, Romania
* Correspondence: nicolae_gtuturas@yahoo.com (N.G.Ţ.); jipa@brahms.fizica.unibuc.ro (A.J.)

Abstract

In order to describe the heavy ion collision dynamics in hot and very dense nuclear matter formed in the overlapping region of the two colliding nuclei, we used simulated numerical calculations for FAIR available energies. We used the anti-k_T jet-detection algorithm for highlighting the main directions of flow in Au-Au collisions at CBM energies, thus obtaining structures of the events depending on the number of flow streams. The jet-finder algorithm identified domains in the y-ψ (rapidity-azimuthal angle) plane, where the number of charged particles, momenta and energy take higher values than in other areas of this plane. The anisotropic flow coefficients v_n may offer information about the pressure gradients in the early stages of the collision and about the high-density nuclear matter properties. The observation of K^+ mesons in heavy ion collisions is of interest since K^+ mesons, due to their strangeness, have a mean free path that exceeds the dimensions of the "fireball". In the numerical calculations the interval of rapidity $0 < y < 0.8$ is highlighted, for which the fluctuations of the antiparticle to particle ratio excitation functions show non-monotonic behavior in the 10-13 A GeV energy interval.

Keywords: hadronic gas; K^+ mesons; anisotropic flow; resonance matter; particle ratios

1. Introduction and Motivation

In nearly eight decades of relativistic and ultrarelativistic heavy ions collisions [1–4], many hopes have been accomplished [5–11]. These collisions help in the understanding of the nuclear matter behaviour in extreme conditions [1–15]. The specific behaviour depends on the thermodynamic equilibrium type, global or local [16,17], and collision geometry [18]. In these efforts, one of the interesting results is the observation of the strong connection between the very hot and dense participant region evolution and the evolution of the Universe after the ”Big Bang” [19,20]. The possibility to have new states of nuclear matter is considered by all laboratories having experimental facilities in this field [1–12,14–20].

New accelerator systems and associated experimental set-ups are in construction in present, to cover better the phase diagram of the nuclear matter and the possible connections with cosmological phenomena, namely: FAIR (**F**acility for **A**ntiproton and **I**on **R**esearch) at GSI Darmstadt (Germany) [21], respectively, NICA (**N**uclotron-based **I**on **C**ollider F**a**cility) at JINR Dubna (Russia) [22]. At BNL, based at RHIC, the **E**lectron-**I**on **C**ollider (EIC) [10,23] is in construction, from January 2020. All of these experiments offer good opportunities for observing and investigating different states of matter at high energies under laboratory conditions.

The dense nuclear and subnuclear matter research program at FAIR will be carried out by the **C**ompressed **B**aryonic **M**atter (CBM) and **H**igh **A**cceptance **DiE**lectron **S**pectrometer (HADES) experiments. These experiments, which are associated with the description of the dynamics of the

 doi:10.20944/preprints202604.1449.v1

relativistic nuclear collisions, will help to identify some phase transitions with the consideration of a transition regime in which certain phases coexist.

The CBM experiment [24,25] is motivated by the study of the equation of state specific to nuclear matter, and by the search of phase transitions, its program being compatible with that of RHIC and LHC. In this experiment it will be possible to create conditions for high and very high baryonic densities, some compatible with the formation of some types of stars, such as neutron stars [24–28]. The objective of the CBM is the measurement of very rare probes (types of particles), including multi-hyperons and hyper-nuclei at measurement rates of up to 10 MHz [25].

2. Results and Discussions

The theoretical models describing the dynamics of relativistic nuclear collisions allow, beyond a conceptual development that continuously diversifies, the creation of links between the experimentally determined physical quantities, the proposed mechanisms and the properties of the newly formed nuclear system in the collisions of relativistic ions. [24,29,30].

The types of flow (collective phenomena) of the nuclear matter formed in relativistic heavy ion collisions have different implications regarding the coverage of the phase space. Thus, for longitudinal and transverse radial flow, it is important to have a high acceptance in rapidity and transverse momentum for different types of particles. Anisotropic flow requires a uniform coverage of the azimuth for the correct reconstruction of the reaction plane. Otherwise, to highlight the existence of a phase coexistence region in the QCD phase diagram, it is necessary to investigate a comprehensive extended set of observables for which we will search the non-monotonous region of their excitation functions. [24,31–36].

In the present work, we chose the AMPT code which is based on a transport model (A Multi-Phase Transport) [29,30], and the UrQMD (Ultrarelativistic Quantum Molecular Dynamics) code [37,38]; these are simulation codes for heavy ion collisions and have over time become reliable tools for interpretation of many processes that occur in this type of phenomenology. The UrQMD code is based on a microscopic model that considers the covariant propagation of hadrons on classical trajectories in combination with stochastic binary scatterings, string formation with color confinement, and resonance decays. The Hydro module introduces an intermediate hydrodynamical evolution for the hot and dense stage of the collision [39]. The AMPT model has been applied to the study of various observables in nuclear collisions such as particle yields, and particle correlations. The model processes the initial conditions of the collisions, the partonic interactions, the conversion of partonic matter into hadronic matter, as well as the hadronic interaction during the final state. The AMPT model can describe the transverse momentum spectra and elliptic flow in the newly nuclear matter formed in the heavy ion relativistic collisions. For the simulations made in this article we used the string fragmentation model and a mechanism for imposing the baryon stopping, known as a "popcorn" type mechanism [29,30].

2.1. Flow Streams Analysis

The analysis of the anisotropic flow can offer information about the density and geometry fluctuations of the participant region of the collision, in agreement with collision centrality. It is in order to recall now some general ideas about the anisotropic flow. The overlapping region formed in a not very central collision is spatially anisotropic, and the back-scattering between the particles converts this spatial anisotropy into a momentum anisotropy. This anisotropy is quantified by the Fourier decomposition of the azimuthal distribution of the particles relative to the reaction plane (defined by the impact parameter vector and the projectile momentum vector):

$$E\frac{d^3N}{dp^3} = \frac{d^2N}{2\pi p_T dp_T dy}\left(1 + 2\sum_n v_n \cos[n(\Phi - \Phi_{RP})]\right) \quad (1)$$

where Φ_{RP} is the azimuthal reaction angle and Φ is the azimuthal angle of a particle (relative to the Laboratory Frame) [24,36].

 doi:10.20944/preprints202604.1449.v1

In our study, we propose an interesting method for the analysis of relativistic nuclear collisions, in particular the anisotropic flow, using notions of nuclear matter jets [40] and flow streams [41], respectively. For the flow stream structure display, a sequential recombination jet finding algorithm [40,41] was applied.

Jet finding algorithms are indispensable tools in high-energy physics, providing the needed link between experimentally measurable observables and the underlying QCD parton-level dynamics. By clustering hadronic final states into jets, these algorithms allow us to enable meaningful comparisons between theory and experiment.

Among the many proposed methods, four algorithms have emerged as the most widely used and robust: SISCone (which belongs to the cone family algorithms) [42], k_T [43], Cambridge–Aachen [44], and anti-k_T [45,46] (residing in the sequential recombination algorithm family). A key property shared by all four of them is infrared and collinear (IRC) safety, ensuring that the definition of jets is stable against soft emissions or collinear splittings - an essential requirement for theoretical consistency.

The sequential recombination algorithms' general clustering procedure is based on defining distance measures between particles i and j :

$$d_{ij} = min(k_{Ti}^{2p}, k_{Tj}^{2p}) \frac{\Delta_{ij}^2}{R^2} \tag{2}$$

and between particle i and the beam B:

$$d_{iB} = k_{Ti}^{2p} \tag{3}$$

where p is the algorithm parameter (p=1 for k_T, p=0 for Cambridge–Aachen, p=-1 for anti-k_T), k_T is the transverse momentum, Δ_{ij} is the distance in rapidity–azimuth space ($\Delta_{ij}^2 = (y_i - y_j)^2 + (\phi_i - \phi_j)^2$, where y_i and ϕ_i are rapidity, and azimuthal angle of particle "i" respectively), and R is the jet radius parameter.

In our computations, we use the anti-k_T algorithm, which is particularly favored for producing geometrically well-defined, conical jets. The procedure is iterative:

1. Compute all d_{ij} and d_{iB}.
2. Find the smallest distance:
   - If it is d_{ij}, merge particles i and j.
   - If it is d_{iB}, declare particle i a jet and remove it from the list.
3. Repeat until no particles remain.

The algorithm, by its construction, will preferentially cluster the soft particles (with small transverse momentum) around the hard ones, resulting in jets with stable shapes. This iterative clustering ensures that the hardest particles act as "seeds", while softer radiation is absorbed into their cones [46,47].

2.1.1. The Flow Streams Method

Since at the energies compatible with the CBM experiment we do not have the so-called "hard scattering" that occurs in HEP (high energy physics: LHC, RHIC) experiments, the formation of jets is, unfortunately, highly unlikely. However, using the above specific algorithms for finding jets at the energies considered by us, we can deduce the existence of a structure similar to jets, which can instead characterize the specific collective flow we're after, which we call "flow streams" [41]. What does this technique bring in addition (new), compared to the traditional Fourier coefficients, which already provide a global characterization of the pressure gradients from the initial stages of the dense matter in the collision zone? Flow streams offer a local and at the same time complementary structural characterization of the collective flow. For example, two events with identical v_2 may nevertheless have very different internal organization - e.g., one may exhibit a single strong flow stream while another has several competing streams - a behavior which is not captured by the traditional Fourier coefficients technique. Notably, as was shown in [41] Fourier coefficients v_n characterizing anisotropic

 doi:10.20944/preprints202604.1449.v1

flow are more distinctly highlighted when analyzing separate event flow shape classes, as opposed to when events are considered in a mixed ensemble - when the Fourier coefficients are mediated over all particles in an event and over all events [48,49].

Flow streams were constructed following the method already introduced in a previous article [41] using the anti-k_T clustering algorithm, with the jet radius parameter R treated as a free variable. A comprehensive parameter scan was performed across multiple values of R to evaluate the robustness and sensitivity of the clustering procedure. Following these investigations, the choice R = 1 was adopted, as it provided a consistent and effective scale for capturing the full extent of the flow stream structures while ensuring methodological convenience. The algorithm was applied event-by-event to all charged particles emitted at midrapidity. As already mentioned, the anti-k_T algorithm was not used for jet reconstruction in the hard-scattering sense, but as a general clustering tool to group soft hadrons into coherent structures that represent dominant directions of transverse collective motion. Neutral particles were excluded, and clusters containing fewer than five charged particles were removed to reduce contributions from statistical fluctuations. The surviving clusters were interpreted as flow streams, as there's also a visual representation of them: regions in rapidity-azimuthal angle, where there's a higher activity in terms of particle fluxes, and their momenta and energies, compared to other areas. Once found, these flow streams are ordered by their total energy (sum of constituent particle energies), with *Stream 1* defined as the most energetic, *Stream 2* the next most energetic and so on. For each stream, its total transverse momentum (which represents the dominant directions of collective transverse motion within the event) was determined from the vector sum of constituent transverse momenta. Since the number of flow streams - also defined as the number of maxima in the angular distribution of charged particles in the transverse plane - varied across events, the events were subsequently classified according to the number of identified streams, providing a compact, topology-based characterization of the event's collective flow structure. By applying the flow-stream technique, we obtained a glimpse into the structures of the events depending on the number of flow streams: events with one flow stream, events with two flow streams or more than two (5 maximum), as we will see next.

2.1.2. The Analysis and the Results

In Figure 1 an "artistic" image of a two flow streams event is presented. The vector sum of particles momenta composing flow stream I is hereinafter referred as "total momentum of the flow stream I", and its projection on the transverse plane of the reaction is called "total transverse momentum of the flow stream I". In this picture I = 1, 2.

 doi:10.20944/preprints202604.1449.v1

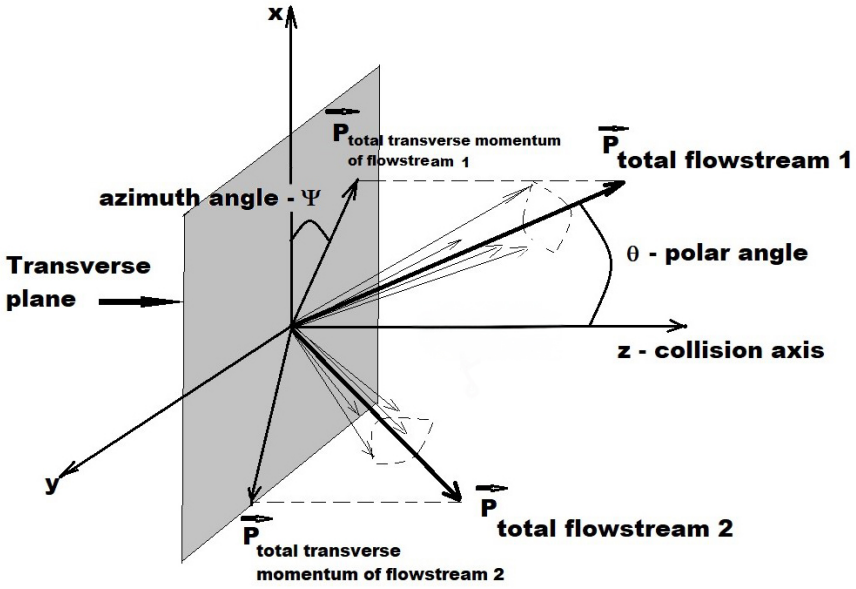

Figure 1. "Artistic" image of a two flow streams event.

In this work, we analyzed Au+Au (in the laboratory frame) reactions with E_{beam} = 4 A GeV (AMPT/UrQMD Hydro).

In the figures below with results of this section, we present different flow streams classes when calculated with azimuthal angle of the transverse momentum of particles (denoted $\Psi_{particles}$) and when we use the azimuthal angle of the total transverse momentum of the flowstream (denoted $\Psi_{P_{T\,flowstreams}}$), with attached tables describing the Fourier fit calculations.

In Figure 2, we can observe that the dominance of the v_3 Fourier coefficient over all other fitted components, combined with the angular separation of the lobes, provides evidence for a 3-flow stream structure. Since the reaction plane geometry is used, this introduces event-by-event smearing. When events are subsequently aligned according to their leading flow-stream direction - following the method introduced by us - the residual event-by-event rotational smearing is eliminated, revealing the underlying flow geometry with better clarity. This is what we precisely see in Figure 3, where the 3-lobed flow is much clearly visible now. The results obtained with the AMPT code are summarized in Figure 4, where we can easily read each Fourier coefficient for the two cases above ($\Psi_{particles}$ and $\Psi_{P_{T\,flowstreams}}$). A comparison with UrQMD/Hydro was also done: the UrQMD prediction for v_3 is clearer than the AMPT, since the v_1, v_2 , v_4, v_5 and v_6 are all aligned around zero (see Figure 4-up). These diversities could be due to the specific properties in the two transport codes (e.g. the existence of a parton phase in the AMPT case compared to the UrQMD code, the hadron phase cross-section interactions, etc - we include some more features that distinguish the mechanisms of the two codes in the second part of the paper). However, in the lower plot of Figure 4, our arguments related to the use of total momentum of flow streams calculated with our method (described in more detail above) are even better emphasized and the differences are blurred: because the rotational smearing was mostly washed out by a judicious choice of the reference plane, as shown by our studies. Here, the error bar has 3 segments to define the range $\pm$ 3 σ. If our results with the two models, UrQMD/Hydro and AMPT are at a distance smaller than 3 standard deviations (3 σ) we have compatibility of the represented Fourrier coefficients. In conclusion, the AMPT and UrQMD/Hydro results are in closer agreement, often even in a compatible range . The same arguments and the same conclusion also hold

 doi:10.20944/preprints202604.1449.v1

and apply for Figures A1 and A2 (please see the Appendix A) which present the quadrangular and pentangular flow shapes, respectively.

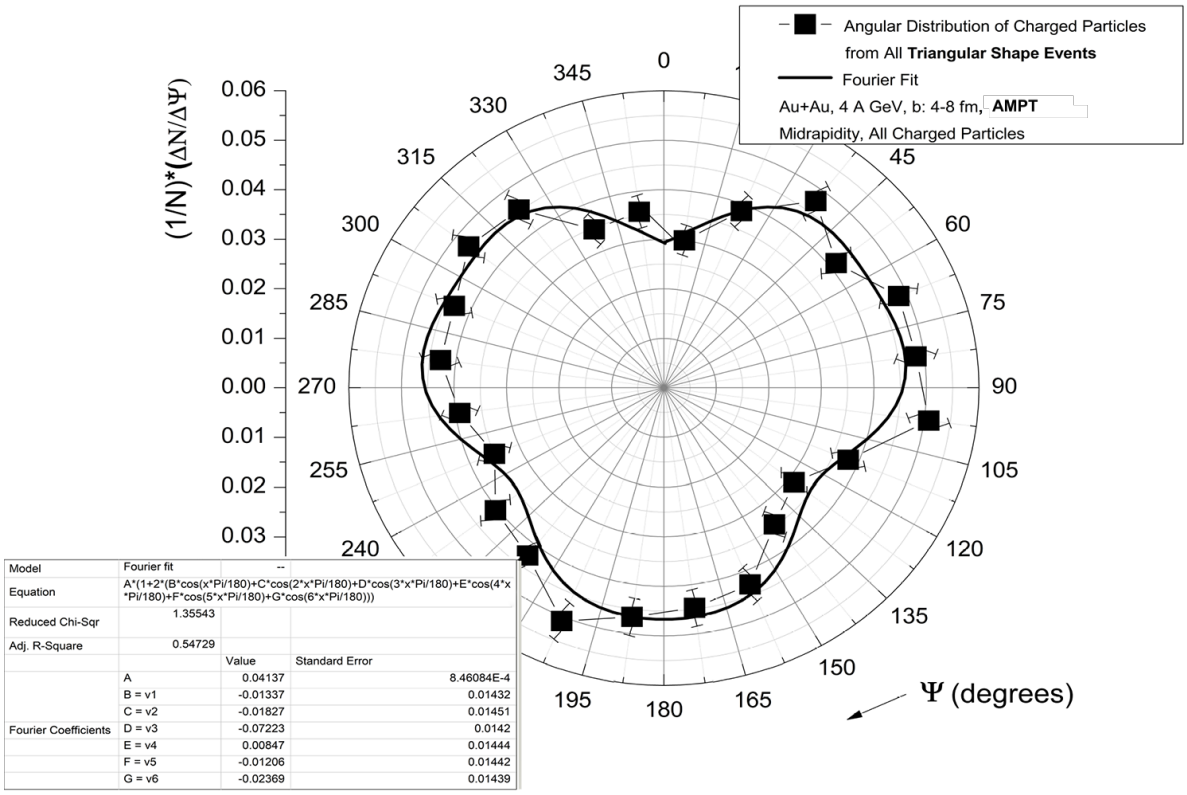

Model	Fourier fit	--	
Equation	A*(1+2*(B*cos(x*Pi/180)+C*cos(2*x*Pi/180)+D*cos(3*x*Pi/180)+E*cos(4*x*Pi/180)+F*cos(5*x*Pi/180)+G*cos(6*x*Pi/180)))		
Reduced Chi-Sqr	1.35543		
Adj. R-Square	0.54729		
		Value	Standard Error
Fourier Coefficients	A	0.04137	8.46084E-4
	B = v1	-0.01337	0.01432
	C = v2	-0.01827	0.01451
	D = v3	-0.07223	0.0142
	E = v4	0.00847	0.01444
	F = v5	-0.01206	0.01442
	G = v6	-0.02369	0.01439

Figure 2. Angular distribution of the transverse momenta of particles from Au+Au at 4 A GeV collisions, AMPT, R = 1, b ∈ [4, 8) fm, midrapidity, triangular- shape structures, and the Fourier fit of the flow streams angular distributions (in the table).

At a beam energy of 4 A GeV, the AMPT transport model generates a remarkably quadrangular flow pattern (Figure 5). This outcome aligns neatly with previously published results [41], which show that quadrangular flow shapes are the most probable across all considered energies and nearly all centrality classes. This quadrangular shape is most probably produced mainly in the initial phases of the collision characterized by a quadrangular eccentricity. We recall here that higher order flow harmonics (n>3) receive contributions not only from the eccentricities in the initial collision stage, which are linear contributions, but also from the lower harmonics interplays, in the form of non-linear mode couplings [49–55]. For v_4 in particular, the non-linear mode coupling is given approximately by half of the square of the elliptic flow value. These considerations apply for the case when the Fourier coefficients are calculated by double-mediation on all particles in one event and then on all events [48], but our procedure is different, by considering event-by-event analysis.

As we do not have sufficient experimental data for the CBM energies (SIS 100), we refer to the results for the nearest energies. As shown by the STAR collaboration and other authors [50,54] the nonlinear component is small for v_4 , compared to the linear component for central collisions, over an extended range of collision energies higher than those discussed in this article , which shows that the initial quadrangular eccentricity is largely responsible for the v_4 behaviour. Then, for the lower energies case, it is expected that the prolonged influence of spectators and the multiple re-scatterings due to the very dense nuclear matter [56,57] will further suppress the development of elliptic component of the flow [51,56]. Studies show ([51] and references within), in general, that v_2 decreases with decreasing collision energy, such that there is small chance for the elliptic flow to completely form for the 4 A GeV

 doi:10.20944/preprints202604.1449.v1

case. Since the nonlinear v_4 component requires a well-developed v_2, which, for low energies, is not realized, most hints still point towards the fact that the harmonic of the fourth order in this regime is dominated by the linear response to the initial ϵ_4 eccentricity. Otherwise, non-flow correlation effects which could add a third term to the higher harmonics ($n > 3$), given by resonance decays and mini-jets fragmentation [48,58] are expected to be small for this energy range [52]. However, considering also the influence of the shear viscosity which has a tendency to increase the non-linear contribution part [49], we would be interested in making a shear viscosity calculation that would show the non-linear contributions more clearly, but this hypothesis requires a separate study.

The same considerations as for the triangular flow streams events hold when considering the leading flow stream as the reference plane (see also Figure A1 from Appendix A for a comparison with the UrQMD/Hydro results).

The observed structure in Figure 6 corresponds more clearly to a 5-flow stream rather than a 4-flow stream, despite the apparent ambiguity in the Fourier fit. Statistically, the measured coefficients $v_4 = 0.15552 \pm 0.01749$ and $v_5 = -0.16706 \pm 0.01743$ are not significantly different, since their difference Δ=0.0015 is smaller than the respective uncertainties. However, the geometry of the event provides stronger evidence: a 4-stream shape has lobes 90° apart, while the actual plot shows narrower lobes separated by about 70°, consistent with five streams. Moreover, flow-shape classification is not determined by Fourier coefficients alone (which are just obtained by fits), but by the number of streams identified via anti-k_T clustering algorithm sorted by flow stream total energy. In this last case (our method), the clustering reveals five distinct streams. As for the changing of the reference plane, the same observations as for Figures 4 and A1 apply: the results obtained with the AMPT and UrQMD/Hydro codes are in good agreement after changing the reference plane to the leading flow-stream (Figure A2). Reiterating the issue of the linear contribution vs the non-linear one (given this time by a combined v_2 and v_3 parts [49,50,55]) of the higher armonics, the same considerations hold as for the quadrangular case: the pentangular eccentricity, for this energy range, is expected to dictate the final form of the pentangular flow shape.

 doi:10.20944/preprints202604.1449.v1

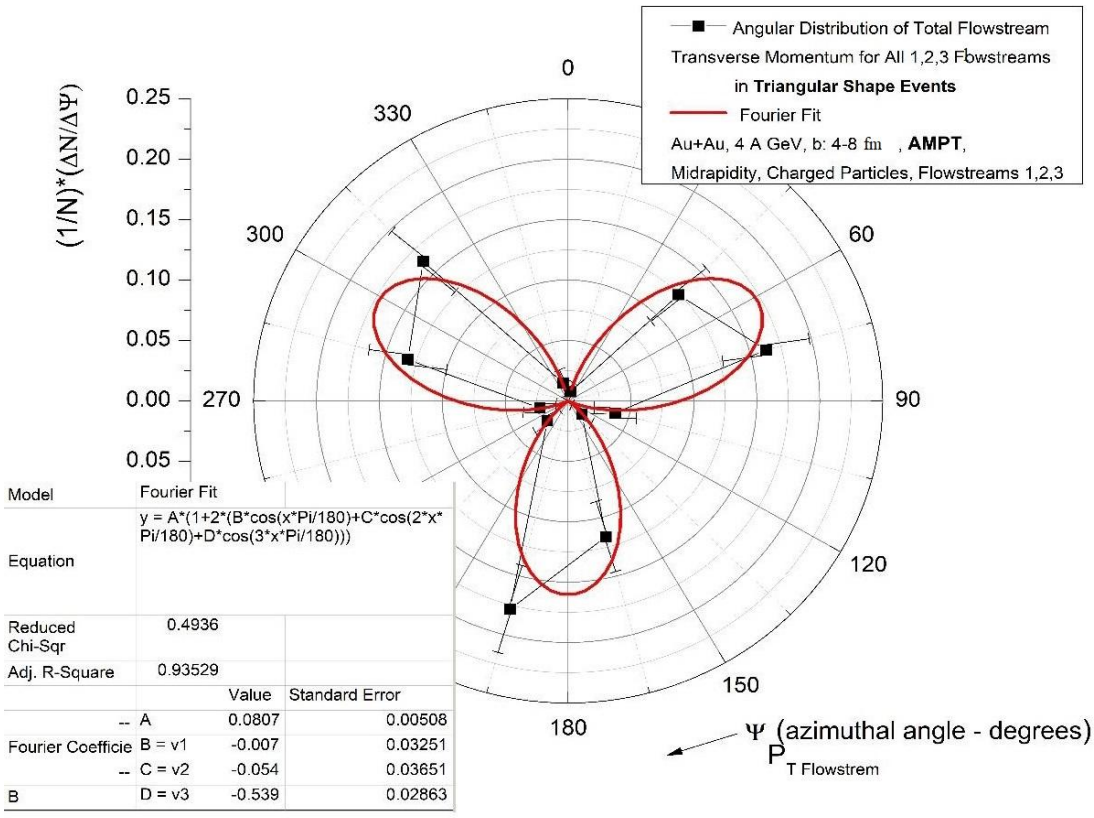

Model	Fourier Fit		
Equation	y = A*(1+2*(B*cos(x*Pi/180)+C*cos(2*x*Pi/180)+D*cos(3*x*Pi/180)))		
Reduced Chi-Sqr	0.4936		
Adj. R-Square	0.93529		
		Value	Standard Error
--	A	0.0807	0.00508
Fourier Coefficie	B = v1	-0.007	0.03251
--	C = v2	-0.054	0.03651
B	D = v3	-0.539	0.02863

Figure 3. Angular distribution of the total transverse momenta of flow streams from Au+Au at 4 A GeV collisions, AMPT, R = 1, b ∈ [4, 8) fm, midrapidity, triangular- shape structures, and the Fourier fit of the flow streams angular distributions (in the table), when the main particle flow streams (flow stream 1) is used as a reference plane.

 doi:10.20944/preprints202604.1449.v1

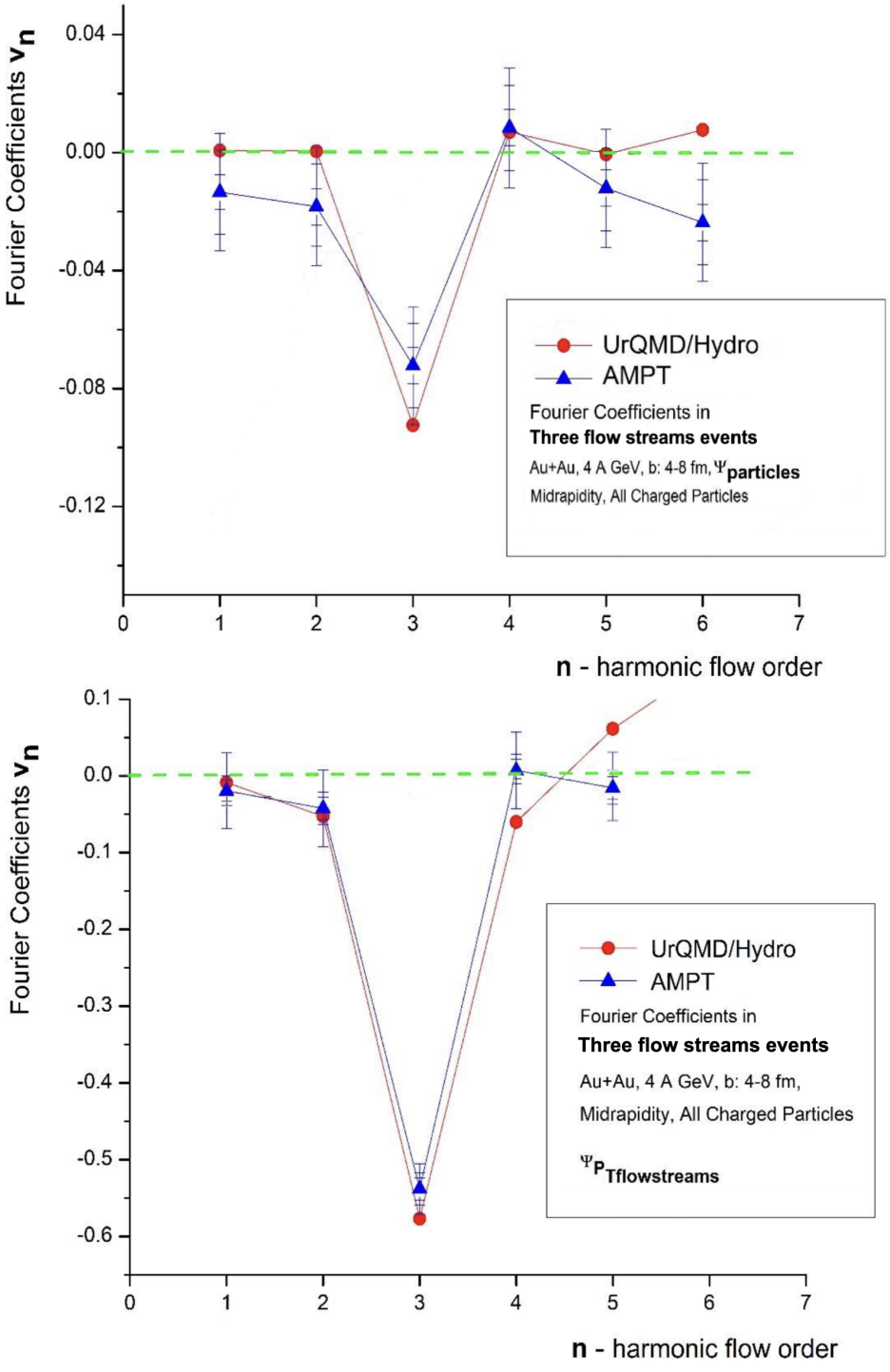

Figure 4. Values of each Fourier coefficient as obtained from fits to p_T distributions in azimuthal angle, when using as the reference plane the reaction plane (up) or the leading flow stream (down), for Au+Au collisions at 4 A GeV, for b $\in$ [4, 8) fm, at mid-rapidity, when only charged particles are used, for 3-flow stream classes. A comparison between the UrQMD/Hydro (red) and AMPT (blue) codes is also shown for every Fourier coefficient.

 doi:10.20944/preprints202604.1449.v1

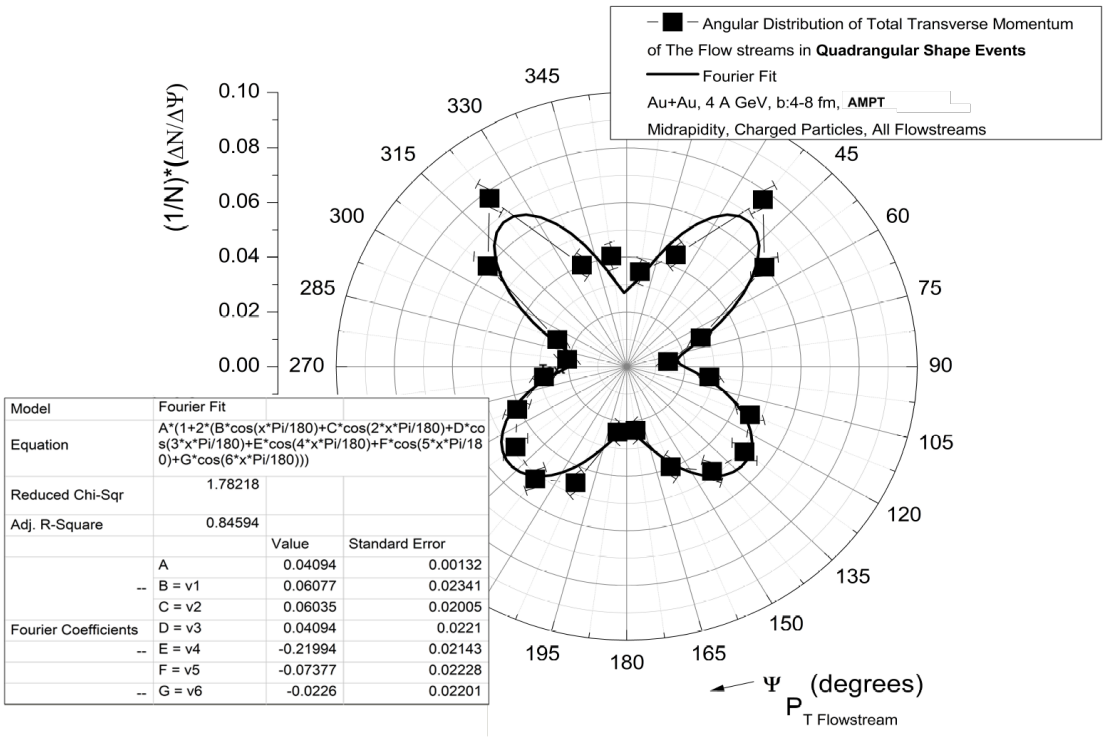

Model	Fourier Fit		
Equation	A*(1+2*(B*cos(x*Pi/180)+C*cos(2*x*Pi/180)+D*cos(3*x*Pi/180)+E*cos(4*x*Pi/180)+F*cos(5*x*Pi/180)+G*cos(6*x*Pi/180)))		
Reduced Chi-Sqr	1.78218		
Adj. R-Square	0.84594		
		Value	Standard Error
Fourier Coefficients	A	0.04094	0.00132
--	B = v1	0.06077	0.02341
	C = v2	0.06035	0.02005
	D = v3	0.04094	0.0221
--	E = v4	-0.21994	0.02143
	F = v5	-0.07377	0.02228
--	G = v6	-0.0226	0.02201

Figure 5. Angular distribution of the total transverse momenta of flow streams from Au+Au at 4 A GeV collisions, AMPT, R = 1, b ∈ [4, 8) fm, midrapidity, quadrangular- shape structures, and the Fourier fit of the flow streams angular distributions (in the table).

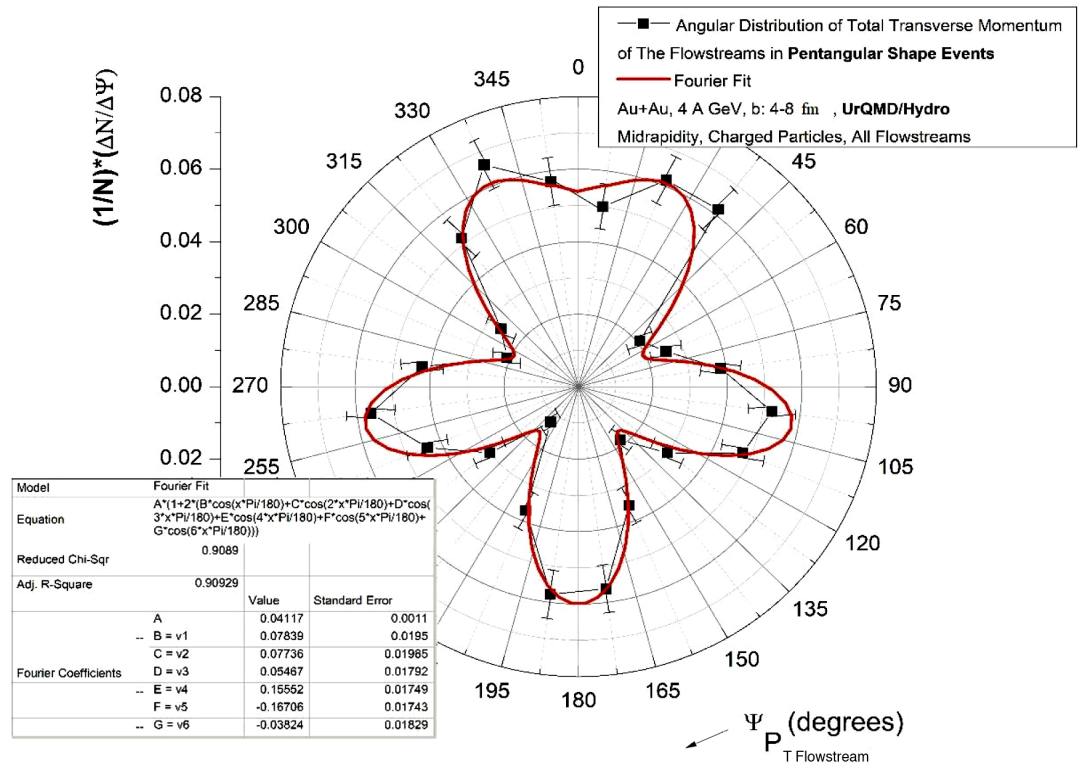

Model	Fourier Fit		
Equation	A*(1+2*(B*cos(x*Pi/180)+C*cos(2*x*Pi/180)+D*cos(3*x*Pi/180)+E*cos(4*x*Pi/180)+F*cos(5*x*Pi/180)+G*cos(6*x*Pi/180)))		
Reduced Chi-Sqr	0.9089		
Adj. R-Square	0.90929		
		Value	Standard Error
Fourier Coefficients	A	0.04117	0.0011
--	B = v1	0.07839	0.0195
	C = v2	0.07736	0.01985
	D = v3	0.05467	0.01792
--	E = v4	0.15552	0.01749
	F = v5	-0.16706	0.01743
--	G = v6	-0.03824	0.01829

Figure 6. Angular distribution of the total transverse momenta of flow streams from Au+Au at 4 A GeV collisions, UrQMD/Hydro, R = 1, b ∈ [4, 8) fm, midrapidity, pentangular- shape structures, and the Fourier fit of the flow streams angular distributions (in the table).

 doi:10.20944/preprints202604.1449.v1

2.2. Antiparticle to Particle Ratio

The excitation functions together with the antiparticle/particle ratios, for a variety of particles, have a remarkable importance in the determination of the "freeze-out" parameters, but also for the elimination of volume fluctuations. The ratios $\frac{K^-}{K^+}$ and $\frac{\bar{p}}{p}$, alongside the other species of particles such as: $\pi^{\pm}$, Λ, $\bar{\Lambda}$, Ξ and $\bar{\Xi}$, allow the study of exotic states (the existence of density isomers) [24,28,31,36,59–65].

The analysis of antiparticle-particle ratios (kaon and proton species) was mainly realized by implementing simulation data obtained with AMPT code. The number of generated events was set to 100000 (and even 1000000, especially in the regions of interest, to thoroughly verify and clarify the quasi-plateau behavior/the results of the initial simulations). Data simulated with the AMPT 2.26t7 codes was used as well, a version of the code which includes string fragmentation and the "popcorn" type mechanism of baryon stopping. We worked with a 0.2 fm/c time step and 150 steps for the hadronic cascade, after which the cascade stops; we tried different beam energies, centrality classes and rapidity ranges, and kept the $0 < y < 0.8$ rapidity interval. For this case, the fluctuations of the excitation function show a non-monotonic behavior in 10-13 A GeV energy interval.

The strangeness, once produced, is conserved throughout the expansion of the hot and dense medium. While no additional strange quarks are created during hadronization, within a good approximation, the apparent yield of strange hadrons may increase as the system converts from partonic to hadronic degrees of freedom. The yields of kaons and antikaons serve as a sensitive probe of strangeness production, since they are the lightest strange mesons and therefore dominate the total strange-particle yield over a wide range of beam energies. Other strange hadrons - such as hyperons (Λ, Ξ, Ω) and the Φ meson - also contribute significantly to the total strangeness content, providing complementary information on the degree of chemical equilibration achieved in the system. At SPS energies, measurements of strangeness production as a function of entropy density reveal a pronounced, abrupt structure that cannot be reproduced by hadronic models. The discrepancy between model predictions and experimental observations has led to the hypothesis that this behavior signals the onset of deconfinement at SPS energies. Consequently, when discussing particle yield ratios at different relativistic collision energies in Au–Au systems, it is essential to also consider the behavior of the antikaon-to-kaon (K^-/K^+) ratio. As a matter of fact, the ratios of particles with the same mass, but with a different content of quarks, such as $\bar{p}/p$, K^-/K^+, are sensitive to the balance between matter and antimatter characterized by baryonic chemical potential. Since the strange quarks are created in the collision, and are not inherited from the interacting nuclei, the degree of equilibrium of the produced fireball can be estimated from the strangeness production [20,24,35,36,66–68].

 doi:10.20944/preprints202604.1449.v1

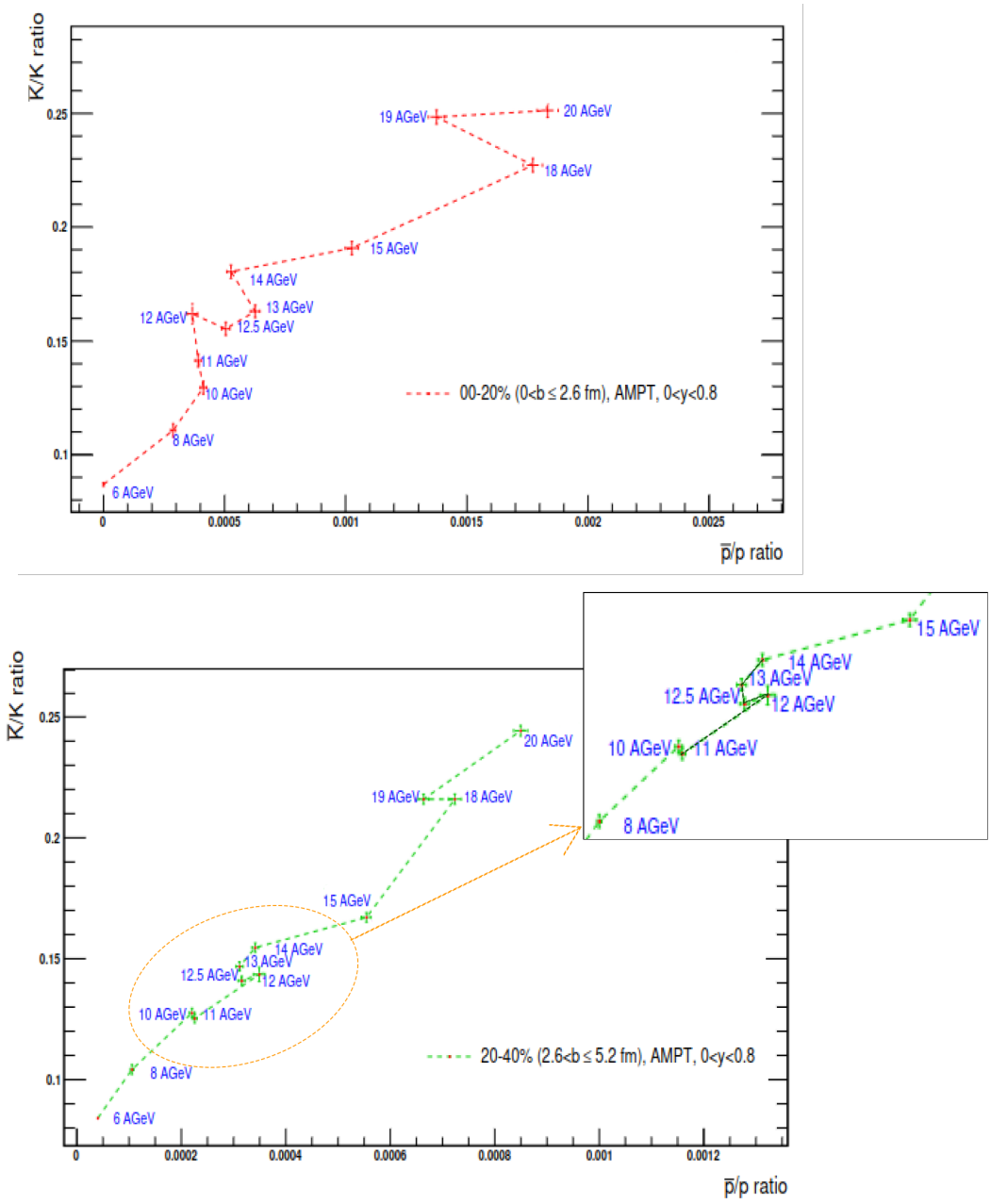

Figure 7. The dependence of the ratio $\frac{K^-}{K^+}$ to the $\frac{\bar{p}}{p}$ ratio, for two centralities for $0 < y < 0.8$ rapidity interval: up) 0-20% centrality class, down) 20-40% centrality class, AMPT code.

In our calculations we can observe, for the $\frac{K^-}{K^+}$ ratio to the $\frac{\bar{p}}{p}$ ratio dependence (please see Figure 7), for two centrality classes, interesting variations, such as short plateaus for three points or quasi-coincident values of the ratios (both on the vertical and horizontal axis), obtained in the range 10-13 A GeV ($\sqrt{s_{NN}} = 4.69$ - $\sqrt{s_{NN}} = 5.29$ GeV) and also in the 18-20 A GeV interval ($\sqrt{s_{NN}} = 6.16$ - $\sqrt{s_{NN}} = 6.48$ GeV). This demonstrates clear enough a non-monotonic behavior. In general, the values of the K^-/K^+ ratio increase with the increase of the collision energy, but we also have regions of the graph where a saturation behavior of the ratio is observed. Thus, we can say that $K^-$and K^+ yields do not have the same growth rate.

We do not have many experiments for such low energies, for a good characterization of K^- production at these energies. At the KaoS experiment, "unusual" variations were observed for the K^-/K^+ ratio up to 2 A GeV: "the antikaon abundance has also been connected to the reduction of the effective antikaon mass via the strength of the strangeness exchange channels with an antikaon in the

 doi:10.20944/preprints202604.1449.v1

final state " [69]. The KaoS collaboration assessed that the inverse slope parameters of the antikaons obtained from transverse spectra are systematically lower than those observed for the kaons [70].

The FOPI and HADES collaborations reported that the fraction of negative kaons originating from the Φ meson feed-down is approximately 20% and therefore is significant [71,72].

The large Φ/K^- ratio reported in [71,72] and the resulting feed-down which gives soft K^- transverse momenta, affects significantly the slope of the K^- and questions the general interpretation of a later freeze-out of the K^- compared to the K^+ [69]. In addition, new mechanisms seem to be required to reproduce microscopically the enhanced Φ production [73,74] . The Φ production is very well known from SPS data; it can be seen that, for the SPS energies, neither the UrQMD nor the HGM models can explain the Φ/π ratio which is given by solid data [75], so efforts must be done in the theoretical area to elucidate the dynamics of Φ particles.

When considering the AMPT code, for example, the hadrons below are added in: for mesons : π, ρ, ω, η, K; and baryons: N, Δ, $N^*(1440)$, $N^*(1535)$, Λ, Σ, Ξ. Among the inelastic channels that appear after baryon-baryon collisions, made available by the ART model within the AMPT code, of particular importance for our study are the kaon production channels: $(N\Delta N^*)(N\Delta N^*) \rightarrow (N\Delta)(\Lambda\Sigma)K$, where the different interaction options between baryons are visible in parentheses [15,29]. One can take into consideration the isospin symmetry breach between particles and antiparticles which depends on the net baryon content. One such effect relevant for kaons is the associated production mechanism $p + p \rightarrow p^+\Lambda^+K^+$ which leads to an increase in the number of positive kaons in the regions where there is an excess of baryons.

In the hadronic gas, some of the channels for the formation of strange particles are the following [24]:

$$\begin{aligned} \pi + \pi &\rightarrow K + \bar{K}, & E_{treshold} &\approx 720\,\text{MeV} \\ \pi + N(\bar{N}) &\rightarrow K(\bar{K}) + \Lambda(\bar{\Lambda}), & E_{treshold} &\approx 540\,\text{MeV} \\ \pi + \Lambda(\bar{\Lambda}) &\rightarrow \Xi(\bar{\Xi}) + K(\bar{K}), & E_{treshold} &\approx 560\,\text{MeV} \\ \pi + \Xi(\bar{\Xi}) &\rightarrow \Omega(\bar{\Omega}) + K(\bar{K}), & E_{treshold} &\approx 705\,\text{MeV} \end{aligned}$$

The AMPT code includes the formation of Φ mesons out of baryon-baryon or meson-baryon scattering channels $(N\Delta N^*)(N\Delta N^*) \rightarrow \Phi NN$, respectively $(\pi\rho)(N\Delta N^*) \leftrightarrow \Phi(N\Delta N^*)$ [76].

The production of antiproton-proton pairs in nucleus-nucleus collision is possible only through multiple collisions and potential collective effects, such as the cumulative effect [4,24,36]. For the production of proton-antiproton pairs, the contribution of $N\Delta$ and $\Delta\Delta$ collisions is very important. The presence of the $N(1440)$ resonance during the production of proton-antiproton pairs is substantial. This contribution slowly drops with the increase in the domain of SIS100 compatible energies [4,24,36]. The above considerations can be recognized in our results for the $\frac{\bar{p}}{p}$ ratio (Figure 7), which does not increase for the 10-12 A GeV range; we observe a minute decrease, but the values of the ratio for this energy interval better display a quasi-plateau. We also remember what the authors of the AMPT code suggest about the results obtained with this code for the K^+/π^+ ratio with a behavior of plateau shape at SPS energies: it approximates a chemical equilibrium [29]. These values of the $\frac{\bar{p}}{p}$ agree with the current experimental data obtained at BES-STAR [77].

We also made calculations (please see Table 1) for the positive and negative kaons temperatures from the inverse of the slope obtained for the transverse momentum distribution fitted with an exponential Boltzman-like function, which implemented the Levenberg-Marquardt minimization algorithm, on a $\frac{1}{2\pi p_T}\frac{d^2N_{ch}}{dyd p_T}$ spectrum [78]. The computations of apparent temperatures calculated for 8, 10, 12 and 14 A GeV in central collisions, are in the same range with the experimental-based data (please see Ref. [79]).

 doi:10.20944/preprints202604.1449.v1

Table 1. Positive and negative kaon apparent temperatures for different collision energies and two centrality classes (AMPT code).

Kaon apparent temperatures [MeV]								
	8 A GeV		10 A GeV		12 A GeV		14 A GeV	
	K^+	K^-	K^+	K^-	K^+	K^-	K^+	K^-
0-20%	177^{+1}_{-1}	181^{+5}_{-5}	186^{+1}_{-1}	182^{+3}_{-3}	185^{+2}_{-2}	202^{+8}_{-8}	193^{+1}_{-1}	197^{+3}_{-3}
χ^2/ndf	1.19	0.92	1.46	1.3	1.32	0.94	1.24	1
20-40%	176^{+1}_{-1}	184^{+3}_{-3}	180^{+1}_{-1}	194^{+3}_{-3}	180^{+1}_{-1}	196^{+3}_{-3}	186^{+1}_{-1}	201^{+2}_{-2}
χ^2/ndf	1.26	0.8	1.35	0.89	1.13	0.81	1.07	0.83

In general, for our calculations, within errors, the apparent temperatures for negative and positive kaons are quite close (we do not see appreciable differences for the inverse slope parameters). There is, however, this exception, at 12 A GeV collision energy, where a higher apparent temperature value is observed for negative kaons (for the 0-20% centrality class). One result which can reinforce the above, is the increased value observed for $\frac{K^-}{K^+}$ ratio depending on the $\frac{\bar{p}}{p}$ ratio, in the same 0-20% centrality class (see Figure 7). This possible connection between the two results at 12 A GeV requires a separate investigation.

Regarding the particle ratios, they have a character of predictions for the future CBM experiment. Thus we made a comparison between the results presented in this article and previous results made with the UrQMD code. We suggest that beyond the interesting similarities in the results obtained with the two codes, different behaviors are still to be expected. In our calculations with the AMPT code, we see a greater variation of the ratio values for the 8-14 A GeV region compared to the values obtained with the UrQMD code in the same energy interval (see Fig. 7 vs Fig. 4 in Ref. [80]).

Concerning the results obtained from both codes, the distribution of the impact parameter differs at large values due to the different implementations of peripheral collisions in the two models [78,81,82]. In our calculations, we divided the generated events into four impact parameter intervals. In the case of the UrQMD code, the distribution contains a relatively larger number of events with a small number of particles, compared to the distributions obtained with the AMPT code. This is in accordance with the distribution of the impact parameter, as it can be observed that the set of events obtained with the UrQMD code contains more peripheral collisions than with the AMPT code [78,81,82]. The π^-/π^+ ratio reflects the degree of balancing of the isospin in the collision, and also the effect of the Coulomb repulsion [24,83]. This ratio values calculated by us with AMPT seem to be less sensitive to the centrality of the collision. In the case of the UrQMD code, the dependence on centrality is evident, the ratio being higher at higher impact parameters (lower collision centrality). Otherwise, the differences tend to flatten out at high energies. These results can indicate the effect of the flow speed of the pions and the Coulomb interaction between the pions and the participating region, for the UrQMD code; otherwise, the AMPT code version that we used doesn't include the Coulomb interaction effect [78,81,82].

Both AMPT and UrQMD codes use an empirical parametrization of the cross-section for $b-\bar{b}$ (baryon-antibaryon) annihilation process. For UrQMD, the cross-section is given by:

$$\sigma_{ann}^{\bar{p}p} = \sigma_0^N \frac{s_0}{s}\left[\frac{A^2 s_0}{(s-s_0)^2 + A^2 s_0} + B\right] \tag{4}$$

where the first term in the bracket refers to the signal Breit-Wigner resonance form and the second term to the background (for details, please see reference [84]).

The following estimation for the AMPT generations was obtained, bearing in mind that the strange baryons are not considered: $\sigma_{\bar{p}p}^{annih} = 67/p_{lab}^{0.7} mb$ [29], where p_{lab} is the proton momentum in the rest frame of the antiproton [29], so UrQMD is wider in comparison to AMPT, in this sense.

 doi:10.20944/preprints202604.1449.v1

We can say, for our calculations, that for UrQMD a better statistics is observed in our results, compared to the the AMPT code, for which sometimes the variations of the values of ratios depending on the energy are larger for the quasi-plateau regions.

Some discussions based on our own simulated data, but also experimental results and model predictions could help to understand what we can see in nucleus-nucleus collisions at FAIR-GSI energies.

3. Conclusions

In the broader context of heavy ion collision studies at the CBM experiment energies, we present a few results based on the simulated data. The anisotropic flow coefficients v_n may offer information about the pressure gradients in the early stages of the collision and about the properties of high-density nuclear matter. The anti-k_T jet finder algorithm, with R = 1, has been used to explore the structure of the event. We present the detected flow shape classes according to the number of maxima in the transverse plane angular distribution. We show the Fourier coefficients v_n of anisotropic flow are better emphasized when we analyze the different event flow shape classes compared to the situation when the events are mixed.

For antiproton-proton to K^-/K^+ ratios inter-dependence, considering different collision energies, our calculations show non-monotonic behavior - for the $0 < y < 0.8$ rapidity interval, 0-20% and 20-40% centrality classes ($0 < b \leq 2.6$ fm and $2.6 < b \leq 5.2$ fm) - in the case of central collisions. This study can be useful for future CBM experimental setups, as well as for the mini-CBM project. These results of the analysis obtained from the simulations are compatible with other results based on different hypothesis, but also with experimental data.

Author Contributions: Conceptualization, N.G.Ţ, Al.J; methodology, N.G.Ţ, Al.J; software, N.G.Ţ, D.A, C.R, A.J, M.A; investigation, Al.J, O.R, M.C, T.E; resources, YaPT system; data curation, O.R, I.L, M.C, T.E; writing—original draft preparation, N.G.Ţ, Al.J, A.J; writing—review and editing, N.G.Ţ, Al.J, A.J; visualization, Al.J, D.A, O.R, I,L, M.C, N.G.Ţ; supervision, Al.J; funding acquisition, Al.J. All authors have read and agreed to the published version of the manuscript.

Funding: This research was funded by FAIR grant number 08/2020 and FAIR-RO/RD/2024

Acknowledgments: This work was supported by IFA, RO-FAIR program,

Conflicts of Interest: The authors declare no conflict of interest.

 doi:10.20944/preprints202604.1449.v1

Appendix A UrQMD/Hydro and AMPT Fourier Coefficients Comparison

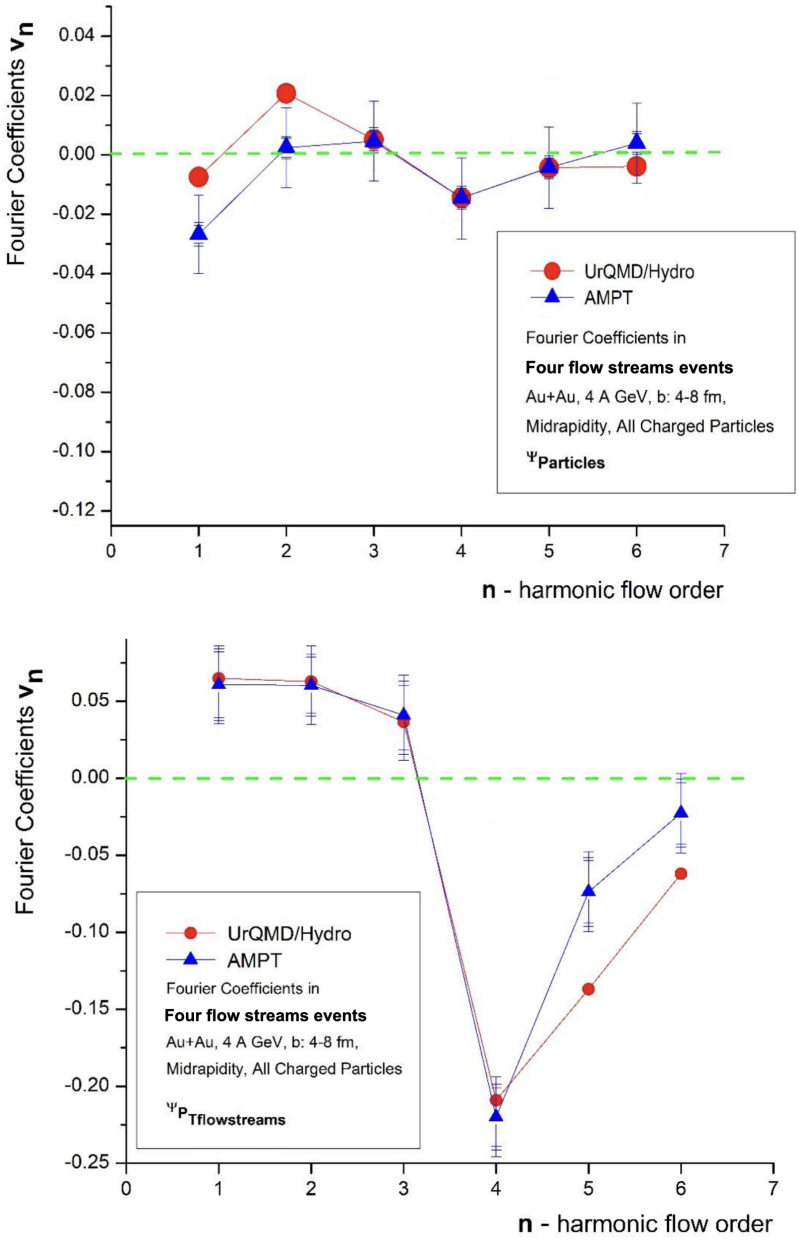

Figure A1. Values of each Fourier coefficient as obtained from fits to p_T distributions in azimuthal angle, when using as the reference plane the reaction plane (up) or the leading flow stream (down), for Au+Au collisions at 4 A GeV, for b $\in$ [4, 8) fm, at mid-rapidity, when only charged particles are used, for four flow streams classes. A comparison between the UrQMD/Hydro (red) and AMPT (blue) codes is also shown for every Fourier coefficient.

 doi:10.20944/preprints202604.1449.v1

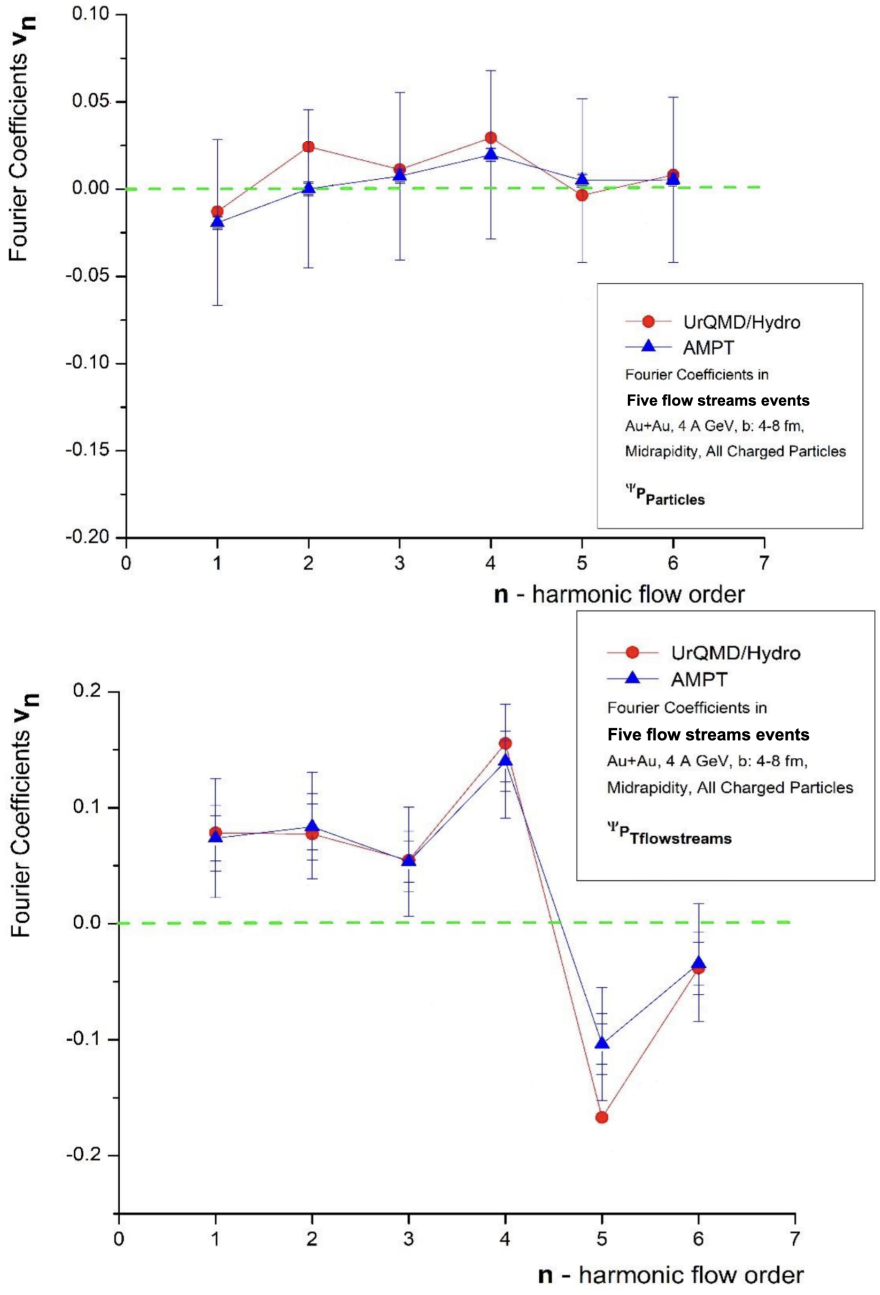

Figure A2. Values of each Fourier coefficient as obtained from fits to p_T distributions in azimuthal angle, when using as the reference plane the reaction plane (up) or the leading flow stream (down), for Au+Au collisions at 4 A GeV, for b $\in$ [4, 8) fm, at mid-rapidity, when only charged particles are used, for five flow streams events class. A comparison between the UrQMD/Hydro (red) and AMPT (blue) codes is also shown for the Fourier coefficients.

References

1. Phyllis Freier, E.J. Lofgren, E.P. Ney, F. Oppenheimer - The heavy component of primary cosmic rays - Physical Review 74(1948)1818-1827; Phyllis Freier, E.J. Lofgren, E.P. Ney, F. Oppenheimer, H.L. Bradt, B. Peters - Evidence for heavy nuclei in the primary cosmic radiation - Physical Review 74(1948)213-217; Phyllis Freier, E.P. Ney, F. Oppenheimer - Cosmic-ray induced nuclear stars at high altitudes - Physical Review 75(1949)1451-1452
2. David Scott - Prog.Part.Nucl.Phys.IV(1981)5
3. S.Goldhaber, H.H.Heckman - Ann.Rev.Nucl.Part.Sci.28(1978)161 E.M.Friedlander, H.H.Heckman - Treatise on Heavy Ion Science - Plenum Press, New York and London, 1984, vol.IV, 460
4. A.M. Baldin - Prog.Part.Nucl.Phys.IV(1981)95
5. Yvonne Leifels for the FOPI Collaboration - Journal of Physics: Conference Series 230 (2010) 012002; Min Sang Ryu, Byungsik Hong, Tae Im Kang, the FOPI Collaboration -FOPI Detector for Heavy-Ion Collision

 doi:10.20944/preprints202604.1449.v1

Experiment at SIS/GSI - J. Korean Phys.Soc. 59(2(3))(2011)1605-1608; P. Achenbach, - New detectors for the kaon and hypernuclear experiments with KaoS at MAMI and with PANDA at GSI – arViv: nucl-ex/0606001 (2006); A. Wagner et al., Evidence for diferent freeze-out radii of high- and low-energy pions emitted in Au+Au collisions at 1 A GeV - Phys. Lett. B 420 (1998) 20-24. H. Weber et al., Hadronic observables from SIS to SPS energies - anything strange with strangeness? - Phys. Rev. C, 2002. nucl-th/0209079.

6. N.Akhababian et al - Preprint IUCN E1-83-670(1983); G.N.Agakhishiev et al - Yad.Fiz.39 (1984)543; C.Beşliu, Al.Jipa - Rev.Roum.Phys.33(1988) 409; C.Beşliu, Al.Jipa - Rom.J.Phys.37 (1992)1011; Al.Jipa - Nucl.Part.Phys.22(1996)231; A.K.Abdurakimov et al – Nucl.Phys.A362(1981)376; M.K.Anikina et al – Z.Phys.C18(1983)109
7. A.Zajc et al - Preprint LBL, LBL-12652 (1982)-350; D.Beavis et al – Phys.Rev.C27(1983) 910; D.Beavis et al – Phys.Rev.C28(1983)2561 A.D.Chacon et al - Phys.Rev.Lett. 60(1988)780
8. Y.Akiba et al (E802 Coll) - Phys.Rev.Lett.70(1993)1057
9. I.G.Bearden et al (NA44 Coll) - Phys.Rev.C58(1998)1656; Eur.Phys.J.C18(2000) 317; Bao-An Li, C.M.Ko, G.Q.Li - Phys.Rev.C50(1994)R2675
10. ***** (RHIC collaborations papers) - Nucl.Phys.A757(2005)1-283, ***** -Nucl.Phys.A994(2020) – proceedings of QM 2019) Lect.Not.Phys.844(2012)1-204
11. H.J.Specht - Prog.Part.Nucl.Phys.XV(1985)479; G.Jarlskog, D.Rein (editors) - Large Hadron Collider Workshop, Aachen, 4-9.X.1990, Preprint CERN CERN 90-10(1990), Preprint ECFA 90-133(1990)
12. F. Becattini et al. - Phys. Rev. Lett. 111, 082302 (2013)
13. Tetyana Galatyuk et al. - Eur. Phys. J. A (2016) 52: 131
14. J. Stachel et al. - J. Phys.: Conf. Ser. 509,012019 (2014)
15. S.Nagamiya-Prog.Part.Nucl.Phys.XV(1985)363; R.Stock-rog.Part.Nucl.Phys.XV(1985)455
16. S.Das Gupta, A.Z.Mekjian - Phys.Rep.72(1981)131; J.J.Molitoris, D.Hahn, H.Stöcker - Prog.Part.Nucl.Phys. XV(1985)239; G.F.Bertsch, S.Das Gupta - 160(1988)189 .
17. L.Landau – Izd.Akad.Nauk SSSR 17(1953)5; .H.Stoecker et al - Phys.Rev.C4(1982)1873; J.Aichelin - Phys.Rep.202(1991)233
18. P.Carruthers, C.C.Shih - Int.J.Mod.Phys.A2(1987)1447 Al.Jipa, C.Beşliu, R.Zaharia, A.M.David - J.Phys.G: Nucl.Part.Phys.22(1996)221
19. ***** - Proceedings of the Quark Matter 2012, 2014, 2018, 2019
20. M.Gyulassy - Prog.Part.Nucl.Phys.XV(1985)403
21. www.gsi.de/fair
22. www.jinr.ru/nica
23. www.bnl.gov/eRHIC, Nucl.Phys.A994(2020) – Proceedings of QM 2019
24. B. Friman et al. (Editors) - The CBM Physics Book – Lecture Notes in Physics 814(2011)
25. The CBM Collaboration - Technical Design Report for the CBM Time-of-Flight System, GSI-2015-01999 (2014); CBM Collaboration - Technical Design Report for the CBM Muon Chambers, GSI-2015-02580 (2015); The CBM Collaboration - Technical Design Report for the CBM Projectile Spectator Detector, GSI-2015-02020 (2015)
26. Alberica Toia – Nucl.Phys. A931(2014)315-319
27. David Blaschke - Lecture Notes in Physics, volume 578, Springer Nature (2001)
28. P. Senger et al – Particles 2(4)(2019)481-490; P. Senger – Particles 2(4)(2019)499-510
29. Z.W. Lin et al - Phys. Rev. C72, 064901(2005); Z.W. Lin et al - Phys. Rev. C64, 011902 (2001); B. Zhang et al - Phys. Rev.C61, 067901 (2000)
30. Zi-Wei Lin, Liang Zheng - arXiv:2110.02989 (2021)
31. Jean Letessier, Johann Rafelski - Hadrons and Quark–Gluon Plasma, Cambridge Press, 2002
32. H.Heiselberg, C.J.Pethick, E.Staubo – Phys.Rev.Lett.70(1993)1355
33. M.Floris – Nucl.Phys. A931(2014)103-112
34. Adam Bzdak, Volker Koch, and Nils Strodthoff - Phys. Rev. C95(2017)054906
35. Ramona Vogt – Ultrarelativistic Heavy-Ion Collisions - Elsevier Science; 1st edition, 2007
36. Al. Jipa, C.Bețliu – Elemens of Rellativistic Nuclear Physics. Course Notes (Elemente de Fizică nucleară relativistă. Note de curs) – University of Bucharest Publishing House (Editura Universității din București), 2002
37. S. A. Bass, M. Belkacem, M. Bleicher, M. Brandstetter, L. Bravina, C. Ernst, L. Gerland, M. Hofmann, S. Hofmann, J. Konopka, G. Mao, L. Neise, S. Soff, C. Spieles, H. Weber, L. A. Winckelmann, H. Stocker, W. Greiner, Ch. Hartnack, J. Aichelin and N. Amelin - Prog. Part. Nucl. Phys. 41 (1998) 225-370

 doi:10.20944/preprints202604.1449.v1

38. M. Bleicher, E. Zabrodin, C. Spieles, S.A. Bass, C. Ernst, S. Soff, L. Bravina, M. Belkacem, H. Weber, H. Stocker, W. Greiner - J. Phys. G: Nucl. Part. Phys. 25 (1999) 1859-1896 or from LANL e-print
39. H. Petersen, Jan Steinheimer, Gerhard Burau, Marcus Bleicher, and Horst Stöcker " Fully integrated transport approach to heavy ion reactions with an intermediate hydrodynamic stage" Phys. Rev. C 78, 044901 2008
40. C.Besliu et al - Eur.Phys.J. A1(1998)65-75
41. D. Argintaru et al. - Eur.Phys.J. A53(1)(2017)6
42. Gavin P. Salam and Grégory Soyez JHEP05(2007)086
43. S. Catani, Y. L. Dokshitzer, M. Olsson, G. Turnock, B.R. Webber - Phys. Lett. B269 (1991) 432-438
44. Yu.L. Dokshitzer et al - JHEP08(1997)001
45. M. Cacciari et al -JHEP04(2008)005
46. M. Cacciari et al. - arXiv:0802.1189v2 [hep-ph]
47. G. C. Blazey et al. - arXiv:hep-ex/0005012v2
48. U. Heinz and R. Snellings - arXiv:1301.2826v1 [nucl-th]
49. D. Teaney and L. Yan - arXiv:1206.1905v2 [nucl-th]
50. STAR Collab, arXiv:2211.11637v2 [nucl-ex]
51. S. Voloshin, A. M. Poskanzer, and R. Snellings arXiv:0809.2949v2 [nucl-ex]
52. STAR Collab, arXiv:1206.5528v1 [nucl-ex]
53. Bhalerao et al, Phys Lett B, 742 (2015) 94-98
54. F. Gardim, arXiv:1111.6538v2 [nucl-th]
55. N. Magdy, Universe 2023, 9, 107
56. C Zhang et al, arXiv:1803.02053v2 [nucl-ex]
57. L. Ma, arXiv:1610.04733v1 [nucl-th]
58. B. Alver, HYSICAL REVIEW C 81, 054905 (2010)
59. H. Sorge - Nuclear Physics A 834(1–4)(2010)237c-240c; A. Andronic, P. Braun-Munzinger, J, Stachel, C. Alt et al. (NA49 Coll) - Phys. Rev.C77(2008)024903; Christof Roland (for the NA49 Collaboration) – J.Phys.G: Nucl.Part.Phys. 31(2005)S1075–S1078
60. D. Adamova et al. (CERES Coll.) - Nucl.Phys. A714(2003)124; I. G. Bearden et al. - Phys.Rev.Lett. 90(2002)102301;
61. Peter Braun-Munzinger, Krzysztof Redlich, Johanna Stachel, J. Cleymans - arXiv:nucl-th/0304013v1 - Particle Production in heavy ion collisions- în 3rd International Conference on Physics and Astrophysics
62. Oana Ristea et al - Romanian Reports in Physics 64(3)(2012)722-727
63. H.Stöcker, W.Greiner – Phys.Rep.137(1986)277
64. J.J.Molitoris, D.Hahn, H.Stöcker - Prog.Part.Nucl.Phys.XV(1985)239; W.Cassing, V.Metag, U.Mosel, K.Niita - Phys.Rep.188(1990)363, V.Metag - International School on Heavy Ion Physics "Solving the Nuclear Paradigm", 6-16.X.1993, Erice, Italy
65. P.Senger - Particles 3(2)(2020)320-335
66. T. Ablyazimov et al - Eur.Phys.J. A53(3)(2017)1-14
67. Cheuk-Yin Wong – Introduction to High-Energy Heavy-Ion Collisions – World Scientific, Singapore, New Jersey, London, Hong Kong, 1994
68. L.P. Csernai – Introduction to Relativistic Heavy-Ion Collisions – Wiley-VCH, Weinheim, Germany, 2008
69. "Strange hadron production at SIS energies: an update from HADES", M. Lorenz et al – for HADES Collaboration – 15'th International Confference Journal of Physics: Conference Series 668 (2016) 012022
70. A. Forster, F. Uhlig, I. Bottcher, D. Brill, M. Debowski et al. - Phys. Rev. C 75 024906 (2007)
71. A. Mangiarotti et al. (FOPI Collaboration) - Nucl. Phys. A714(2003)89
72. G. Agakishiev et al. (HADES Collaboration), Phys. Rev. C 82, 044907 (2010)
73. B. Tomasik and E. E. Kolomeitsev - Acta Phys. Polon. Supp. 5 201 (2012)
74. B. Kampfer, R. Kotte, C. Hartnack, J. Aichelin - J. Phys. G 28 2035 (2002)
75. V. Friese - EPJ Web of Conferences 164, 06004 (2017)
76. B. A. Li and C. M. Ko, Phys. Rev. C 52, 2037 (1995)
77. BES Results from RHIC-STAR - CPOD2021, March 15th-19th, 2021
78. N.G.Țuțuraș – PhD Thesis, University of Bucharest, Faculty of Physics, 2023
79. M.I. Gorenstein, M. Gazdzicki, K. Bugaev - arXiv:hep-ph/0303041v1 5 Mar 2003; Yuliia Balkova, for NA61/SHINE collaboration https://www.epj-conferences.org/articles/epjconf/pdf/2022/15/epjconf_hyp2022_02013.pdf; C.Alt et al - https://arxiv.org/pdf/0710.0118
80. N.G. Țuțuraș et al – Rom.Rep.Phys.71(2019)303, N.G. Țuțuraș et al - CBM Progress Report (2018)173

 doi:10.20944/preprints202604.1449.v1

81. S.Cioranu et al – Romanian Reports în Physics 67(3)(2015)819-830
82. Silviu Cioranu PhD thesis 2013 University of Bucharest
83. Na49 Collaboration - Eur.Phys.J.C 2 (1998) 661-670
84. P. Koch, C.B. Dover - Phys. Rev. C 40, 145 – Published 1 July, 1989